



Optics Letters

Microsphere-assisted super-resolution polarized light microscopy for polarization-sensitive materials

RAN YE,^{1,4,†}  XIANGYU ZHANG,^{1,†} LINGJIE ZHI,¹ YURONG CAO,¹  SORIN MELINTE,²
ZENGBO WANG,³  AND SONGLIN YANG^{1,*} 

¹School of Computer and Electronic Information, Nanjing Normal University, Nanjing 210046, China

²Institute of Information and Communication Technologies, Electronics and Applied Mathematics, Université Catholique de Louvain, Louvain-la-Neuve 1348, Belgium

³School of Computer Science and Engineering, Bangor University, Bangor LL57 1UT, UK

⁴ran.ye@njnu.edu.cn

[†]These authors contributed equally to this work.

*slyang@njnu.edu.cn

Received 26 November 2024; revised 24 December 2024; accepted 26 December 2024; posted 2 January 2025; published 24 January 2025

Polarization sensitivity is a fundamental phenomenon observed in nature, and its application is vital for advancing scientific discoveries. Here, we present a microsphere-assisted polarized light microscopy method that enables high-quality, label-free super-resolution imaging of polarization-sensitive materials. We investigated the imaging performance of this method using various samples, including colloidal crystals and grating structures. Both simulations and experiments were performed to explore the underlying physical mechanisms driving the enhancement in imaging quality. The results of this work have potential values for the fields of polarized light microscopy and super-resolution imaging. © 2025 Optica Publishing Group. All rights, including for text and data mining (TDM), Artificial Intelligence (AI) training, and similar technologies, are reserved.

<https://doi.org/10.1364/OL.550156>

The diffraction limit represents a fundamental barrier in conventional optical microscopy, restricting lateral resolution to half the wavelength of the illumination. Several methods have been proposed to overcome this barrier, including as structured illumination microscopy [1], superlenses [2,3], and computational microscopic imaging [4,5]. It has been demonstrated that lateral resolution beyond the diffraction limit can be achieved by depositing microspheres on the sample surface [6]. The application of microsphere-assisted super-resolution imaging for confocal imaging [7], biological imaging [8,9], and spectral imaging [10,11] demonstrates its advantages such as low cost, ease of use, and eliminating the need for fluorescent dyes. Imaging mechanisms for microspheres have been linked to the near-field evanescent wave [12], photonic hooks [13,14], photonic nanojets (PNJs) [15,16], and other mechanisms [17].

A PNJ is a focused spot formed on the shadow side of the microsphere by illuminating light projected onto the microsphere. They have waists smaller than the diffraction limit and propagate over several optical wavelengths without significant diffraction [18]. PNJs generated by microspheres have been applied on nanopatterning [19], optical inspection [20], and

spectrum measurement [21]. Another important characteristic of PNJs is polarization invariance [22]. It is reported that the PNJ generated by microspheres is basically in the same direction of polarization as that of the incident light, making it possible to perform polarized light illumination in a microsphere-assisted imaging system.

Birefringence is an inherent property of many natural and artificial materials [23]. Polarized light microscopy provides unique insights for analyzing the structures with polarization sensitivity. By measuring changes in polarization state, we can investigate the birefringent properties of anisotropic samples at the molecular level. Polarized fluorescence microscopy has been extensively used for single-molecule observations of both material and biological structures [24]. However, label-free super-resolution imaging of these structures presents challenges. In this Letter, we present a microsphere-assisted super-resolution polarized light microscopy (MS-PM) technique, which achieves high-quality super-resolution imaging for polarization-sensitive materials with the help of polarized PNJs. We applied this technique to various samples, demonstrating its superior performance over conventional microsphere-assisted unpolarized microscopy (MS-uPM). The polarization of PNJs was also theoretically and experimentally studied in this work.

As illustrated in Fig. 1(a), the MS-PM system consists of a microsphere lens integrated with a polarized light microscopic imaging system. To demonstrate the compatibility of the proposed technique with conventional optical microscopes, we employed a commercially available light microscope (Axio Imager.A2m, Carl Zeiss) in this study. The microscope is equipped with a fixed polarizer (453264, Carl Zeiss) and a rotatable analyzer (428103, Carl Zeiss). A halogen lamp (HAL 100, Carl Zeiss) was installed in the setup to provide white-light illumination with a central wavelength of 550 nm. For the microsphere lenses, we chose spherical barium titanate glass (BTG) particles due to their wide application in super-resolution microscopy. The BTG particles were purchased from Microspheres-Nanospheres (USA) and have a refractive index of ~ 1.90 and a diameter of around 20 μm . In the experiments, the microsphere lenses were placed

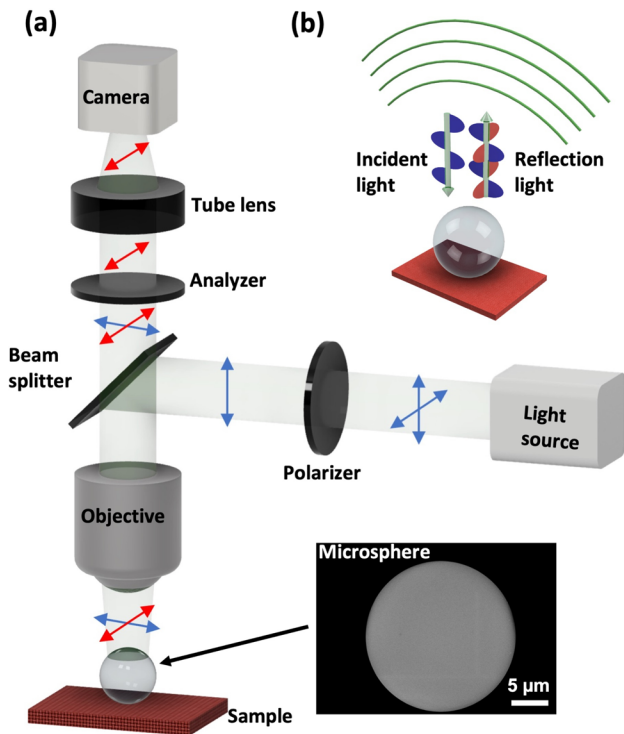


Fig. 1. (a) Diagram of the microsphere-integrated polarized light microscope (MS-PM), the inset on the right is the scanning electron microscopic (SEM) image of a barium titanate glass (BTG) microsphere. (b) Schematic drawing to show the polarization of the incident and reflection light.

in contact with the observation samples, forming a magnified real image above the sample surface. A 20× objective (0.40 NA, EC Epiplan, Zeiss) was used to capture these images. The resolution of the objective is ~ 688 nm, as calculated with Abbe's equation: $R = \lambda/2NA$, where λ is the wavelength of illumination and NA is the numerical aperture of the objective. Finally, optical microscopic images were recorded using a high-speed scientific complementary metal-oxide-semiconductor (CMOS) camera (DFC295, Leica) for further analysis.

The principle of the MS-PM method combines the super-resolution capabilities of microspheres with the contrast-enhancing capabilities of polarized light microscopy. As shown in Fig. 1(b), in a polarized light imaging system, light interacts with the sample and undergoes polarization changes based on the material properties. The analyzer, positioned before the camera, blocks unaltered light and transmits only the light that has undergone polarization changes caused by the sample. By setting the polarizer and analyzer orthogonally, the system isolates the light that has experienced polarization changes, highlighting subtle differences in the sample's interaction with light. This maximizes contrast in the image by selectively allowing light with the desired polarization state to pass through. The role of the microsphere lens is to collect the near-field high-frequency signals and transfer them to the objective, so the resolution of the optical microscope can be enhanced [17].

To demonstrate the advantages of the MS-PM method over MS-uPM, the imaging performance of BTG microspheres was

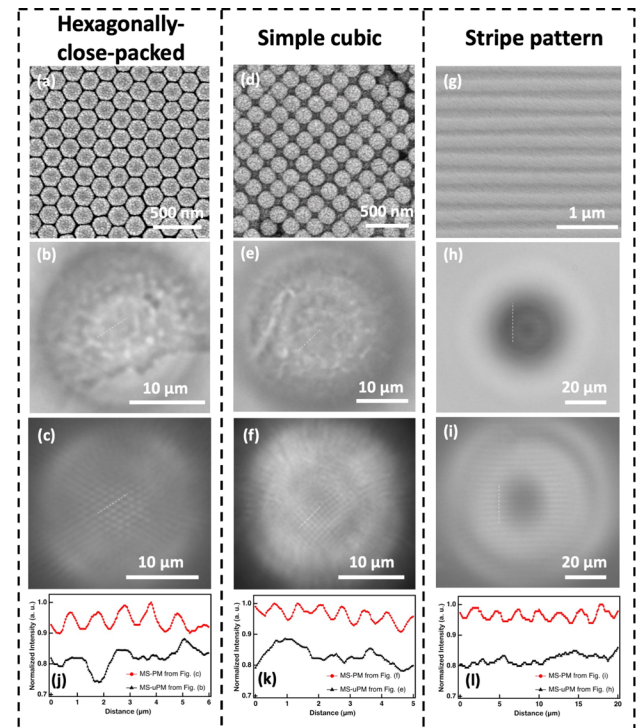


Fig. 2. (a) and (d) SEM images of silica particle arrays with (a) hexagonally close-packed (hcp) structures and (d) simple cubic structures; (g) SEM image of a BD disk; (b), (e), and (h) optical microscopic images of the (b) hcp structures, (e) simple cubic structures and (h) stripe patterns obtained with MS-uPM; (c), (f), and (i) microscopic images of the same structures obtained with MS-PM. (j)–(l) Intensity profiles across the dash lines in the corresponding images.

compared under polarized and unpolarized microscopy conditions, with the polarizer and analyzer aligned orthogonally for polarized microscopy. The first sample we used is 200-nm-diameter silica particle arrays with hexagonally close-packed (hcp) structures [Fig. 2(a)]. This sample was prepared from colloidal suspensions (Nanorainbow, China) using a gravity-assisted self-assembly method [25]. Before observation, we coated the sample with 10-nm-thick Ag films via physical vapor deposition to enhance its optical reflectance. As shown in Fig. 2(b), we cannot see hcp structures through the BTG microsphere with MS-uPM. However, when we switched to MS-PM and observed the same region, the silica particles can be clearly resolved, and the structure of their arrangement became visible [Fig. 2(c)]. As shown in Figs. 2(d)–2(f), for samples with simple cubic structures, the MS-PM technique again shows a better imaging performance than the MS-uPM. The corresponding intensity profiles [Figs. 2(j) and 2(k)] further validate the improved image contrast. In addition, the MS-PM technique also demonstrates an improved performance for naturally birefringent calcite particles (Fig. S1 in Supplement 1).

Blu-ray disks (BDs) are a common popular observation sample in super-resolution imaging due to their commercial availability and sub-wavelength microstructures. As shown in Fig. 2(g), the BD has a stripe pattern with 200-nm-wide tracks and 100 nm gap between two adjacent tracks. These dimensions exceed the resolution limit of our imaging system (0.40 NA objective). Figures 2(h) and 2(i) show microscopic images of

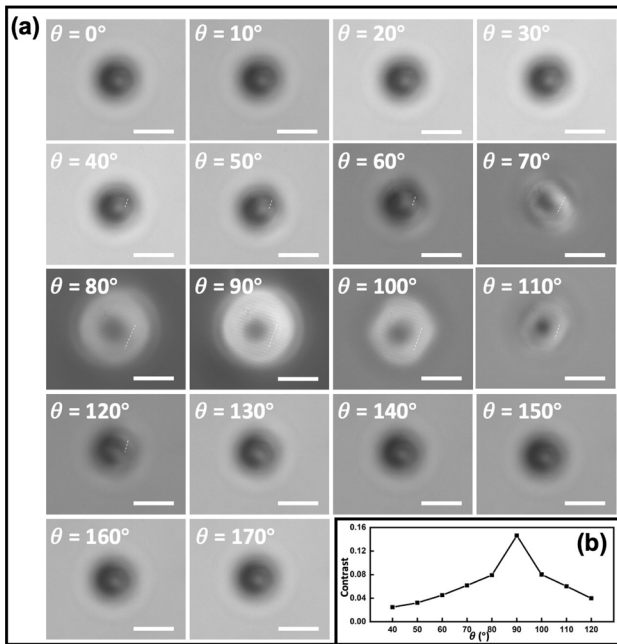


Fig. 3. (a) MS-PM images of stripe patterns obtained when the angle (θ) between the polarizer and analyzer increases from 0° to 170° . The scale bars are $10 \mu\text{m}$. (b) Imaging contrast of the MS-PM as a function of the angle θ .

the BD obtained using the MS-uPM and MS-PM techniques, respectively. The imaging region and the sample stage position remained unchanged. We found that the MS-PM technique provides higher imaging quality than the MS-uPM. This is also confirmed by the intensity profiles of the corresponding images [Fig. 2(l)].

Then, we investigated the effect of the angle between the axes of the polarizer and analyzer on the imaging performance of MS-PM. We firstly define this angle as θ . As shown in Fig. 3(a), the θ was gradually increased from 0° to 170° in steps of 10° , and microscopic pictures were recorded with a $20\times$ objective at each step. We can see that changes in the angle θ have a significant impact on the performance of the imaging system. The stripe pattern cannot be observed when the analyzer is parallel to the polarizer ($\theta = 0^\circ$) or when the angle between them is small ($\theta \leq 30^\circ$). The pattern becomes gradually more visible as we increase the θ from 30° to 90° by rotating the analyzer. The highest imaging quality is achieved when the analyzer is perpendicular to the polarizer ($\theta = 90^\circ$). Increasing the θ further from 90° to 120° results in a decline in imaging quality, and the stripe pattern finally becomes invisible when θ exceeds 120° . The field of view (FOV) gradually increases and then decreases as θ increases, with an optimal FOV of $\sim 28 \mu\text{m}^2$ and a magnification of $\sim 3\times$ obtained when θ is 90° . The angle between the polarizer axis and BD stripe also affects the observed stripe pattern, with the best contrast obtained when the angle is close to 45° (Fig. S2 in Supplement 1).

In order to quantitatively analyze the above results, we use the formula below to calculate the contrast of images:

$$\text{Contrast} = \frac{I_{\max} - I_{\min}}{I_{\max} + I_{\min}},$$

where I_{\max} and I_{\min} are the maximum and minimum grayscale values of the stripe pattern, respectively. For θ smaller than 40° or

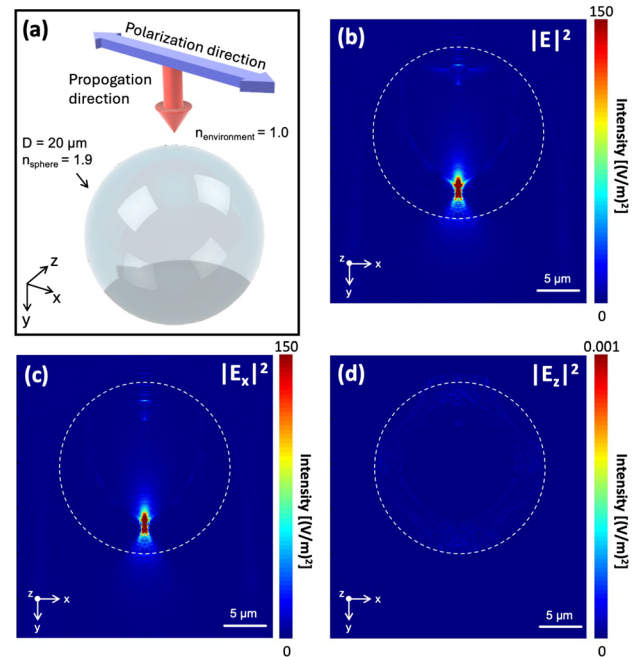


Fig. 4. (a) Schematic drawing of the model for the 3D simulation of light field. (b) Simulated light field generated by a microsphere under polarized light irradiation. (c) X-component of the light field. (d) Z-component of the light field.

larger than 120° , no contrast can be obtained since the pattern is not visible. As shown in Fig. 3(b), the imaging contrast increases gradually from 0.025 to 0.144 as θ increases from 40° to 90° . The contrast decreases to 0.041 when θ is further increased from 90° to 120° . The contrast reaches a maximum of 0.144 when θ reaches 90° , which corresponds to the perpendicular alignment of the axes of the polarizer and analyzer.

The finite-difference time-domain (FDTD) method is widely used to theoretically analyze the light field generated by microspheres. As shown in Fig. 4(a), we used the three-dimensional FDTD method to investigate the polarization of the PNJ of BTG microspheres. The microsphere, with a $20 \mu\text{m}$ diameter and a refractive index (n_{sphere}) of 1.90, is illuminated by 550 nm plane waves polarized along the x axis and propagating along the y axis. The refractive index of the surrounding environment is set to be the same as air ($n_{\text{environment}} = 1.00$). Figure 4(b) shows the simulated $|E|^2$ intensity of the light field, showing an intensity enhancement inside the microsphere (red color). The maximum intensity of the light field is 2809.84 (V/m)^2 . Figures 4(c) and 4(d) are the X-component ($|E_x|^2$) and Z-component ($|E_z|^2$) of the simulated light field, respectively. The $|E_x|^2$ exhibits a significantly higher intensity than the $|E_z|^2$. The maximum intensity of $|E_x|^2$ is 2781.74 (V/m)^2 , which is about 99% of the maximum intensity of $|E|^2$, indicating that the polarization state of the incident light remains basically unchanged when propagating through the microsphere.

In addition, experiments were performed to demonstrate the generation of polarized PNJs from microspheres. To the best of our knowledge, this is the first study to experimentally demonstrate the polarization of PNJs. The setup for polarized PNJ measurement is based on a transmission microscopic imaging system [Fig. 5(a)]. During experiments, plane waves from a white-light source were first polarized by a linear polarizer and

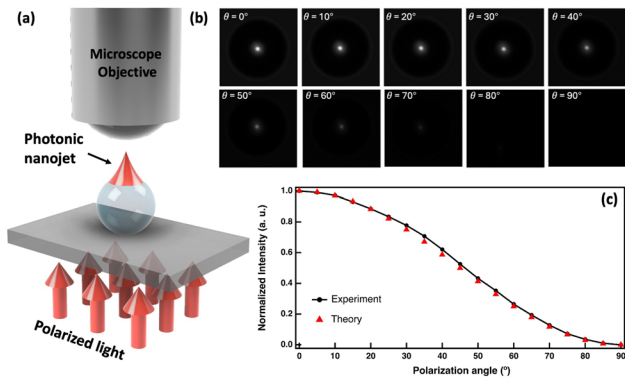


Fig. 5. (a) Schematic drawing of the experimental setup to demonstrate the polarization of PNJs. (b) Pictures of the polarized PNJs obtained when the analyzer was rotated gradually from 0° to 90° . (c) Maximum intensity of the polarized PNJ as a function of the rotation angle of the analyzer.

then propagated through a 20- μm -diameter BTG microsphere from the bottom. The microsphere was on a commercial soda-lime glass microscope slide (No. 7101, Sail Brand, China). On the other side of the microsphere, we used a 50 \times , 0.75 NA microscope objective to capture the PNJ formed by the microsphere. A rotatable analyzer was positioned after the objective to determine the polarization of the PNJ. The intensity of the PNJ was measured by a CMOS camera.

As shown in Fig. 5(b), we can observe the PNJ as a bright spot in the recorded images. The intensity of the PNJ decreases as the angle between the polarizer and analyzer axes increases. The maximum intensity is achieved when the polarization axis of the analyzer is in parallel with that of the polarizer ($\theta = 0^\circ$). The PNJ gradually dims as the angle θ increases from 0° to 90° . Finally, the PNJ cannot be seen in the camera when the polarizer and analyzer are perpendicular to each other ($\theta = 90^\circ$).

Then, the intensity change of the PNJ was quantified by measuring the grayscale value of the bright spot. Figure 5(c) shows the intensity of PNJ as the function of the θ angle. The theoretical intensity in the figure is calculated using Malus's law: $I_t = I_0 \cdot \cos^2 \theta$, where I_t is the intensity of the light transmitted through the analyzer, I_0 is the incident polarized light intensity, and θ is the angle between the polarizer and analyzer axes. We found that the experimentally measured data (black dots) is in good agreement with the theoretical values (red triangles), indicating that the PNJ of the microsphere is primarily linearly polarized, and the polarizing axis of the PNJ is same as that of incident light.

In conclusion, we have developed a microsphere-based super-resolution polarized light microscopy method in this work, which can significantly enhance the imaging performance of conventional optical microscopes for polarization-sensitive objects by generating polarized PNJs from dielectric microspheres. The polarization of PNJs has been theoretically and experimentally confirmed. The imaging performance of the method has been demonstrated using various polarization-sensitive materials with hcp, simple cubic, and stripe structures. These findings contribute to advancements in polarized light microscopy and super-resolution imaging.

Funding. National Natural Science Foundation of China (62105156); Royal Society (IEC\R2\202178); BU-IA Award (S46910); Belgian Fonds de la Recherche Scientifique-FNRS (T.0126.22, U.N027.18).

Disclosures. The authors declare no conflicts of interest.

Data availability. Data underlying the results presented in this Letter are not publicly available but may be obtained from the authors upon reasonable request.

Supplemental document. See Supplement 1 for supporting content.

REFERENCES

- J. Qian, Y. Cao, Y. Bi, *et al.*, *eLight* **3**, 4 (2023).
- J. B. Pendry, *Phys. Rev. Lett.* **85**, 3966 (2000).
- N. Fang, H. Lee, C. Sun, *et al.*, *Science* **308**, 534 (2005).
- Y. Shu, J. Sun, J. Lyu, *et al.*, *PhotonIX* **3**, 24 (2022).
- L. Lu, J. Li, Y. Shu, *et al.*, *Adv. Photonics* **4**, 056002 (2022).
- Z. Wang, W. Guo, L. L. B. Luk'yanchuk, *et al.*, *Nat. Commun.* **2**, 218 (2011).
- Y. Yan, L. Li, C. Feng, *et al.*, *ACS Nano* **8**, 1809 (2014).
- H. Yang, N. Moullan, J. Auwerx, *et al.*, *Small* **10**, 1712 (2013).
- A. Trukhova, M. Pavlova, O. Sinityna, *et al.*, *J. Biophotonics* **15**, e202200078 (2022).
- Y. Li, C. Qiu, H. Ji, *et al.*, *Adv. Opt. Mater.* **11**, 2300172 (2023).
- J. Park, Y. Choi, S. Kwon, *et al.*, *Light: Sci. Appl.* **13**, 122 (2024).
- Y. Ben-Aryeh, *J. Opt. Soc. Am. A* **33**, 2284 (2016).
- Q. Shang, F. Tang, L. Yu, *et al.*, *Photonics* **8**, 513 (2021).
- P. Zou, C. Xu, L. Zhi, *et al.*, *IEEE Photonics Technol. Lett.* **36**, 353 (2024).
- H. Yang, R. Trouillon, G. Huszka, *et al.*, *Nano Lett.* **16**, 4862 (2016).
- S. Yang, F. Wang, Y.-H. Ye, *et al.*, *Opt. Express* **25**, 27551 (2017).
- L. Chen, Y. Zhou, Y. Li, *et al.*, *Appl. Phys. Rev.* **6**, 021304 (2019).
- Z. Chen, A. Taflove, and V. Backman, *Opt. Express* **12**, 1214 (2004).
- Z. B. Wang, W. Guo, A. Pena, *et al.*, *Opt. Express* **16**, 19706 (2008).
- J. Zhu, J. Liu, T. Xu, *et al.*, *Int. J. Extrem. Manuf.* **4**, 032001 (2022).
- S. Kwon, J. Park, K. Kim, *et al.*, *ACS Photonics* **11**, 32 (2022).
- P. B. Johnson, A. Karvounis, H. J. Singh, *et al.*, *Optica* **8**, 674 (2021).
- M. Chen, F. Fan, S.-T. Xu, *et al.*, *Sci. Rep.* **6**, 38562 (2016).
- A. M. Vrabioiu and T. J. Mitchison, *Nature* **443**, 466 (2006).
- C. Fang, S. Yang, X. Wang, *et al.*, *Colloid Interface Sci. Commun.* **37**, 100286 (2020).